Metadata of the chapter that will be visualized in SpringerLink

Book Title	Magnesium Technology 2024	
Series Title		
Chapter Title	Thermodynamics of Mg–Y–O Alloys and Segregation at the Mg/MgO Interface	
Copyright Year	2024	
Copyright HolderName	The Minerals, Metals & Materials Society	
Corresponding Author	Family Name	**Schmid-Fetzer**
	Particle	
	Given Name	**Rainer**
	Prefix	
	Suffix	
	Role	
	Division	
	Organization	Institute of Metallurgy, Clausthal University of Technology
	Address	Robert-Koch-Str. 42, 38678, Clausthal-Zellerfeld, Germany
	Division	
	Organization	Institute of Metallurgy, Clausthal University of Technology
	Address	Robert-Koch-Str. 42, 38678, Clausthal-Zellerfeld, Germany
	Email	schmid-fetzer@tu-clausthal.de
Author	Family Name	**Wang**
	Particle	
	Given Name	**Shihao**
	Prefix	
	Suffix	
	Role	
	Division	SuperSTEM Laboratory
	Organization	SciTech Daresbury Campus
	Address	Daresbury, WA4 4AD, UK
	Email	swang@superstem.org
Author	Family Name	**Fan**
	Particle	
	Given Name	**Zhongyun**
	Prefix	
	Suffix	
	Role	
	Division	
	Organization	BCAST, Brunel University London
	Address	Uxbridge, UB8 3PH, Middlesex, UK
	Email	Zhongyun.Fan@brunel.ac.uk

Abstract

Elemental segregation driven by the reduction of the total Gibbs energy of the system has been widely observed at the melt/substrate interfaces in various Al- and Mg alloys containing different inoculant particles. This study provides experimental observations, analyses, and identifications of the formation of Y-segregation 2DCs at the Mg/MgO interfaces in a solidified Mg–0.5Y (w%) sample. From an extended Gibbs adsorption isotherm, the interfacial segregation of solute Y in a dilute Mg alloy melt is quantitatively described. The thermodynamics of the elemental interactions, conditions for the formation of MgO and Y_2O_3 particles, and the contributions to the interfacial energy difference are detailed. A reasonable atomic segregation factor at the liquid/MgO interface from the bulk Mg–0.5Y melt is estimated. This changes the structural and chemical configuration at the interface, thus the nucleation potency of native MgO particles as well as the as-cast grain size.

Keywords (separated by '-') Thermodynamics - Nucleation potency - Grain refinement - ICME

Thermodynamics of Mg–Y–O Alloys and Segregation at the Mg/MgO Interface

Rainer Schmid-Fetzer, Shihao Wang, and Zhongyun Fan

Abstract

Elemental segregation driven by the reduction of the total Gibbs energy of the system has been widely observed at the melt/substrate interfaces in various Al- and Mg alloys containing different inoculant particles. This study provides experimental observations, analyses, and identifications of the formation of Y-segregation 2DCs at the Mg/MgO interfaces in a solidified Mg–0.5Y (w%) sample. From an extended Gibbs adsorption isotherm, the interfacial segregation of solute Y in a dilute Mg alloy melt is quantitatively described. The thermodynamics of the elemental interactions, conditions for the formation of MgO and Y_2O_3 particles, and the contributions to the interfacial energy difference are detailed. A reasonable atomic segregation factor at the liquid/MgO interface from the bulk Mg–0.5Y melt is estimated. This changes the structural and chemical configuration at the interface, thus the nucleation potency of native MgO particles as well as the as-cast grain size.

Keywords

Thermodynamics • Nucleation potency • Grain refinement • ICME

Introduction

This study on elemental segregation driven by the reduction of the total Gibbs energy provides experimental observations, analyses, and identifications of the formation of Y-segregation two-dimensional-compounds (2DCs) at the Mg/MgO interfaces in a solidified Mg–0.5Y (wt.%) sample. It is shown that the segregation of Y occurs in the Mg–0.5Y melt, forming specifically Y_2O_3 2DC at the liquid-Mg/$\{111\}_{MgO}$ interface and Mg(Y)–O 2DC monolayer at the liquid-Mg/$\{100\}_{MgO}$ interface. That is proven by dedicated electron microscopy, and a summary is depicted in Fig. 1 [1].

This changes the nucleation potency of native MgO particles as well as the as-cast grain size. That is demonstrated by grain refinement of commercially pure Mg treated by high shear melt conditioning, HSMC, before casting (CP Mg-HSMC), shown as a basis in Fig. 2, left-hand micrographs. Segregation of Y towards the highly dispersed native MgO particles in the melt after addition of 0.5 wt.% Y is suggested to improve the observed grain refinement in Mg–0.5Y–HSMC, Fig. 2, right-hand micrographs. The average as-cast grain size is reduced from 235 ± 18 µm to 106 ± 4 µm [1]. The grain refining mechanism is attributed to the enhanced potency of {111} MgO particles (the predominant oxide in terms of population) modified by Y_2O_3 2DC, their dispersity and abundant number density, and the necessary growth restriction provided by 0.5 wt.% Y.

Thermodynamics and Interfacial Energy

The thermodynamics of the elemental interactions, conditions for the formation of MgO and Y_2O_3 particles, and the contributions to the interfacial energy difference are detailed below. From an extended Gibbs adsorption isotherm, the interfacial segregation of solute Y in a dilute Mg alloy melt is quantitatively described [1, 2]. It is suggested that

R. Schmid-Fetzer (✉)
Institute of Metallurgy, Clausthal University of Technology, Robert-Koch-Str. 42, 38678 Clausthal-Zellerfeld, Germany
e-mail: schmid-fetzer@tu-clausthal.de

S. Wang
SuperSTEM Laboratory, SciTech Daresbury Campus, Daresbury, WA4 4AD, UK
e-mail: swang@superstem.org

Z. Fan
BCAST, Brunel University London, Uxbridge, UB8 3PH, Middlesex, UK
e-mail: Zhongyun.Fan@brunel.ac.uk

A. Leonard et al. (eds.), *Magnesium Technology 2024*, The Minerals, Metals & Materials Series,
https://doi.org/10.1007/978-3-031-50240-8_35

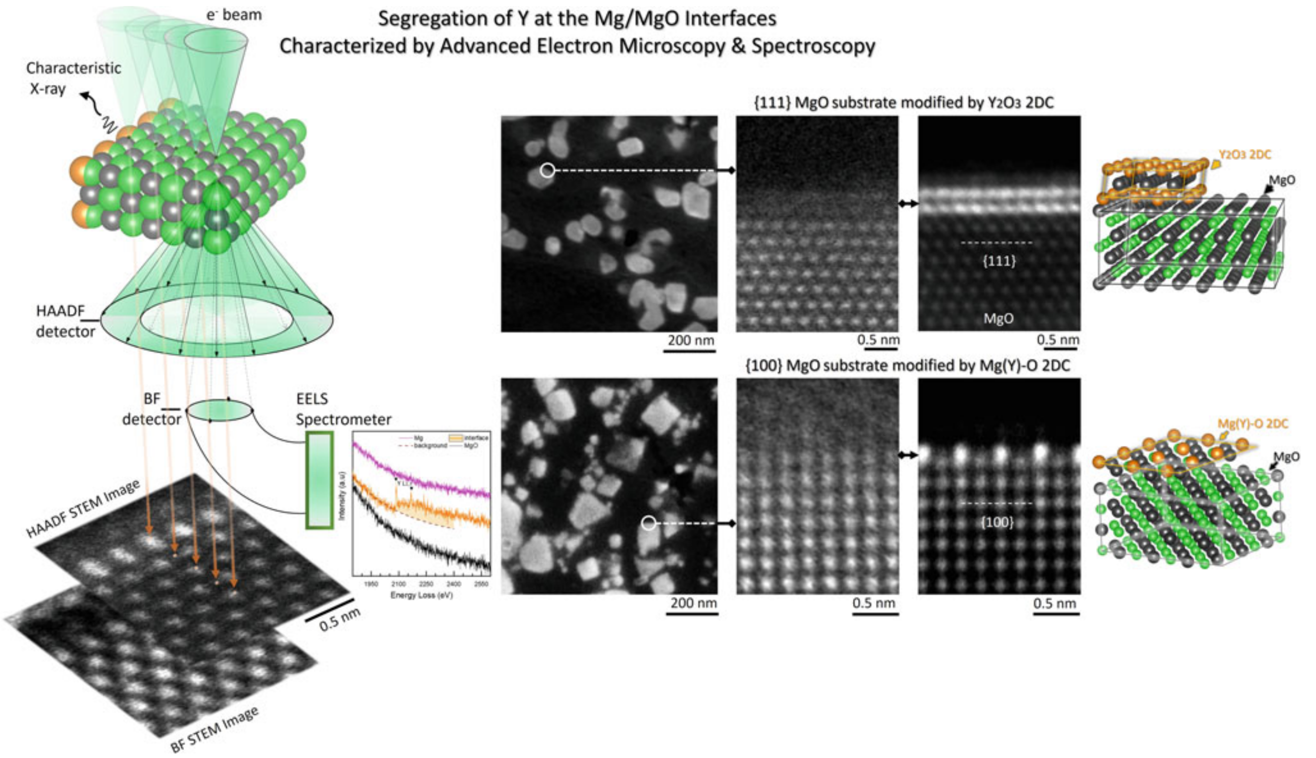

Fig. 1 Graphical sketch of the electron microscopic methods and results to determine and distinguish the Y_2O_3 2DC at the liquid-Mg/$\{111\}_{\mathrm{MgO}}$ interface and Mg(Y)–O 2DC monolayer at the liquid-Mg/$\{100\}_{\mathrm{MgO}}$ interface [1]

interfacial segregation is favored by (1) a negative difference in interfacial energies approximated by $\Delta\gamma = \gamma^i_{\mathrm{Y(L)/MgO}} - \gamma^i_{\mathrm{Mg(L)/MgO}}$ in this case, (2) a positive interaction term Ω of a regular solution between solvent and solute atoms related to a positive enthalpy of mixing $\Delta_{\mathrm{mix}}H^{\mathrm{Liquid}}_{\mathrm{Mg-Y}}$, and (3) a positive difference in entropies of fusion between pure solvent and solute $\Delta S^i = \Delta_{\mathrm{fus}}S_{\mathrm{Mg}} - \Delta_{\mathrm{fus}}S_{\mathrm{Y}}$. The three contributions are considered separately below.

Enthalpy and Entropy Contributions

A strong attractive interaction among Mg and Y in the melt is proven to exist from a comprehensive CALHAD assessment of that binary system [3] and the following data is calculated from these thermodynamic parameters using the Pandat software [4, 5]. A large negative value of the mixing enthalpy with the minimum value of $\Delta_{\mathrm{mix}}H^{\mathrm{Liquid}}_{\mathrm{Mg-Y}} = -10.6\,\mathrm{kJ/mol}$ at 41 at.% Y is obtained from the subregular solution [3]. The approximation by a regular solution equation to fit the dilute, Mg-rich range results in $\Delta_{\mathrm{mix}}H^{\mathrm{Liquid,reg}}_{\mathrm{Mg-Y}} = -14\,\mathrm{kJ/mol}$ at 50 at.% Y, corresponding to the interaction term $\Omega = -56$ kJ/mol. This strong negative term impedes the interfacial segregation of Y. The coordination numbers $Z_l = 9$, $Z_V = 12$, $Z = 13$, in the notation of Ref. [2], are used for the numerical calculations. Although the value of the entropy difference, $\Delta S^i = 2.837\,\mathrm{J/mol/K}$ calculated from Ref. [3], is positive it only accounts for a small promotional contribution to the interfacial segregation of Y. At 700 °C its contribution is about 18 times smaller compared to the impeding Ω term.

Interfacial Energy Contributions

The remaining impeding effect can be canceled if the value of $\Delta\gamma$ is negatively large enough. The interfacial energies of pure liquid elements/MgO are not known. However, the difference $\Delta\gamma$ can be predicted by solving Eq. (25) in Ref. [2] with the data given above. At 700 °C the limit is $\Delta\gamma < -1.05\ \mathrm{J/m^2}$ to result in enrichment of Y. The value of $\Delta\gamma = -1.39\ \mathrm{J/m^2}$ is obtained for reasonable atomic segregation of factor 10 with 1.37 at.% Y (4.8 wt.% Y) at the Liquid/$\{111\}_{\mathrm{MgO}}$ interface from the bulk 0.137 at.% Y (0.5 wt.% Y) melt.

The sign of $\Delta\gamma$ may be estimated to check the plausibility of assuming $\Delta\gamma < -1.05\ \mathrm{J/m^2}$. Clearly, the interface Mg(L)/MgO is non-reactive, whereas strong reactions are expected at the Y(L)/MgO interface as shown later by inspection of

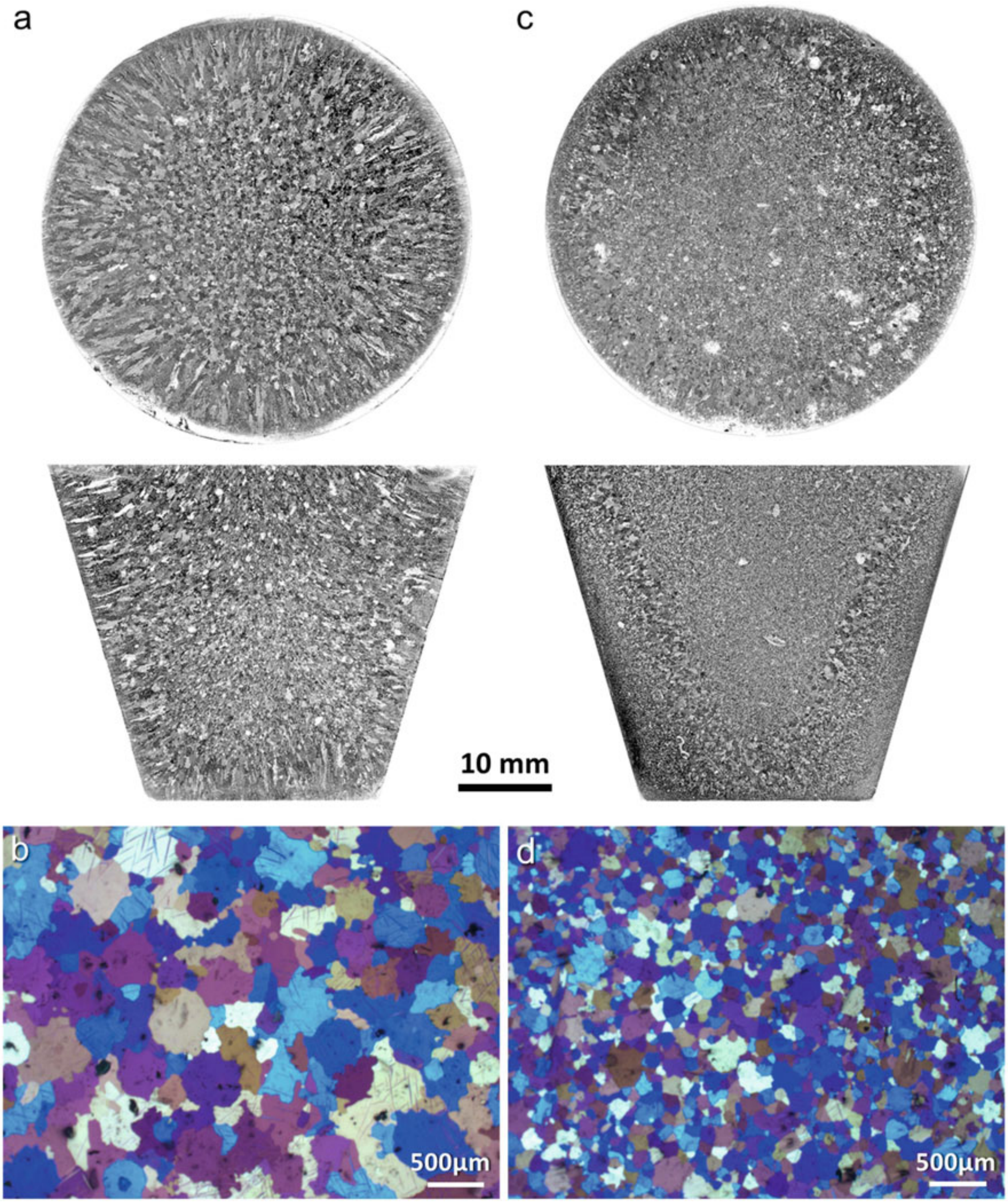

Fig. 2 Grain size of commercially pure Mg with highly dispersed native MgO particles, CP Mg–HSMC, left-hand micrographs (**a**, **b**), is significantly reduced by the addition of 0.5 wt.% Y enabling segregation of Y in Mg–0.5Y–HSMC right-hand micrographs (**c**, **d**). Both melts were treated by high shear melt conditioning, HSMC, before casting [1]

the Mg–Y–O phase diagram. If interfacial reactions occur in metal/oxide systems, the interfacial energies and wetting are difficult to analyze [6] but, in general, the wetting tendency and work of adhesion are increased significantly compared to the non-reactive case [7].

The work of adhesion, $W_{\mathrm{X}}^{\mathrm{ad}}$, is the work against surface forces required to separate the pure liquid element X from a ceramic substrate such as MgO. It is related to the three interfacial energies involved, $\gamma^{i}_{\mathrm{MgO/vapor}}$, $\gamma^{i}_{\mathrm{X(L)/vapor}}$, and $\gamma^{i}_{\mathrm{X(L)/MgO}}$ [7]:

$$W_{\mathrm{X}}^{\mathrm{ad}} = \gamma^{i}_{\mathrm{MgO/vapor}} + \gamma^{i}_{\mathrm{X(L)/vapor}} - \gamma^{i}_{\mathrm{X(L)/MgO}} \quad (1)$$

and to the experimentally determined contact angle θ

$$W_{X}^{ad} = \gamma^{i}_{X(L)/vapor}(1 + \cos\theta) \quad (2)$$

Therefore, the difference in work of adhesion of reactive Y(L), $W_{Y}^{ad-react}$, ~~,~~and non-reactive Mg(L), $W_{Mg}^{ad-Non-react}$, on MgO is given as

$$W_{Y}^{ad-react} - W_{Mg}^{ad-Non-react} = \gamma^{i}_{Y(L)/vapor} - \gamma^{i}_{Mg(L)/vapor} + \gamma^{i}_{Mg(L)/MgO} - \gamma^{i}_{Y(L)/MgO} \quad (3)$$

Inserting the difference in interfacial energies of the condensed phases, $\Delta\gamma = \gamma^{i}_{Y(L)/MgO} - \gamma^{i}_{Mg(L)/MgO}$, we obtain

$$W_{Y}^{ad-react} - W_{Mg}^{ad-Non-react} = (\gamma^{i}_{Y(L)/vapor} - \gamma^{i}_{Mg(L)/vapor}) - \Delta\gamma \gg 0 \quad (4)$$

Assuming that the difference in surface tensions, the term in the brackets in Eq. (4), is not dominant compared to $\Delta\gamma$ we obtain at least $\Delta\gamma < 0$, as required to cancel the remaining impeding effect on Y-segregation detailed above. The value of $\Delta\gamma = -1.39$ J/m^2 related to a reasonable atomic segregation of factor 10 may not be quantitatively precise as it depends on the accuracy of input data and assumptions in the model. It is emphasized that a significant Y-segregation towards the Liquid/MgO interface from the bulk Mg–0.5Y melt is verified experimentally [1]. This changes the structural and chemical configuration at the interface, thus the nucleation potency of native MgO particles as well as the as-cast grain size.

Thermodynamics and Phase Diagram

The thermodynamic conditions for the formation of bulk Y_2O_3 particles in Mg–0.5Y, are revealed by the isothermal section at 700 °C and ambient pressure of the Mg–Y–O ternary equilibrium phase diagram. Figure 3 is calculated using Pandat and the PanMg database [4]. The oxygen solubility in liquid-Mg shown in the magnified Mg-rich part in Fig. 3b was verified by the detailed analysis of the experimental phase diagram and thermodynamic data [8]. It shows that the bulk Mg–0.5Y liquid alloy is saturated at 0.24 wt.% O with MgO. This small oxygen content is readily picked up from the ambient during melting because of the extremely low partial pressure of O_2, $p(O_2) = 5 \times 10^{-54}$ bar, calculated at the tie line Liquid + MgO. Therefore, MgO is the only stable native oxide in that Mg–0.5Y alloy which is also observed experimentally. This tie line also proves that the interface Mg(L)/MgO is non-reactive whereas no tie line exists from MgO to any Y-rich liquid indicating that strong reactions are expected at the Y(L)/MgO interface, as stated above. More than 3.9 wt.% Y in the liquid alloy is required to expect Y_2O_3 as the stable bulk oxide. The liquid phase from 3.9 to 46 wt.% Y is in equilibrium with Y_2O_3. It is interesting to note that under the assumed segregation of factor 10 with 4.0 wt.% Y in the liquid monolayer at the Liquid/$\{111\}_{MgO}$ interface one could obtain a local three-phase equilibrium with Y_2O_3 at that interface.

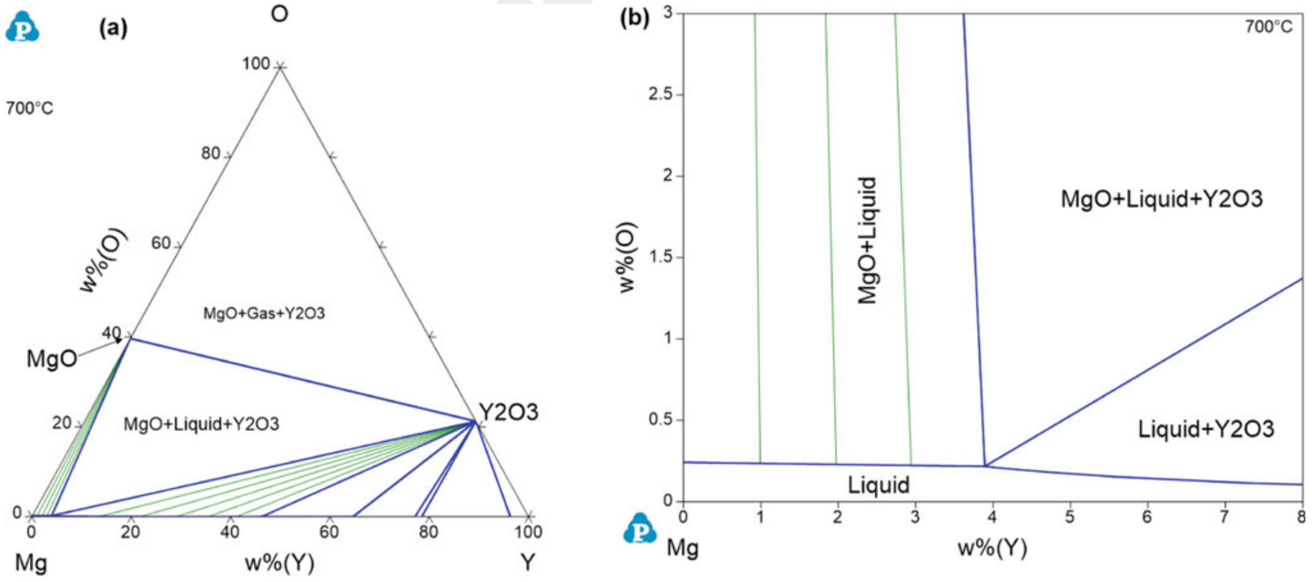

Fig. 3 Isothermal section at 700 °C of the Mg–Y–O equilibrium phase diagram calculated by Pandat and PanMg: **a** complete composition range and **b** Mg-rich corner with Y content up to 8 wt.%

Solidification Simulations

Finally, solidification simulations of the Mg–0.5Y–0.24O (wt.%) alloy, which is just saturated with MgO at 700 °C according to Fig. 3b, reveal the expected solid phases. The results obtained using the Pandat software are shown in Figs. 4 and 5.

Under equilibrium conditions, Fig. 4a, a tiny phase fraction of up to 0.2% of MgO grows from 700 to 647 °C due to the retrograde oxygen solubility in Liquid. From 647 to 643 °C, the bulk of (Mg) solid solution (Hcp) is formed (phase fraction from 0 to 99.27%) together with the growth of MgO from 0.2 to 0.73%. Solidification terminates in this monovariant eutectic reaction, Liquid → (Mg) + MgO at 643 °C without reaching an invariant ternary eutectic.

The distribution of solute Y between Liquid and (Mg) in Fig. 4b starts at the initial 0.5 wt.% in Liquid and increases rapidly from 0.5 to 2.3 wt.% Y during the bulk crystallization of (Mg). The (Mg) solid solution hosts from 0.1 to 0.5 wt.% Y in that secondary step from 647 to 643 °C. Only the two-phase equilibrium (Mg) + MgO exists from 643 to 490 °C. At 490 °C the solubility of 0.5 wt.% Y at the apex of the three-phase equilibrium (Mg) + MgO + Y_2O_3 is attained. Here we have a similarity to the 3.9 wt.% Y in the

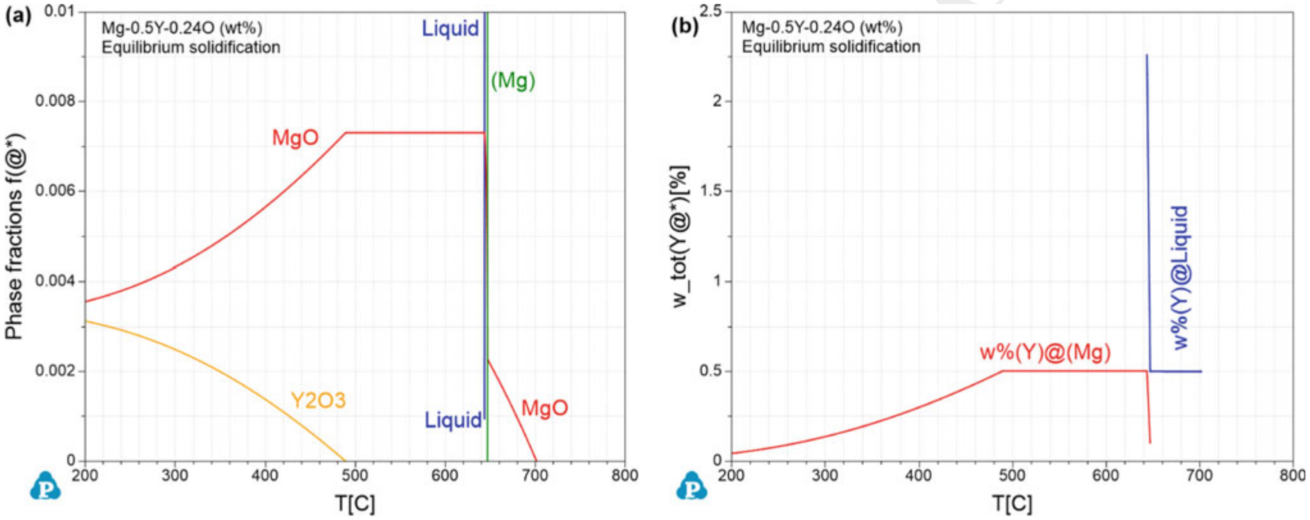

Fig. 4 Solidification simulation of the Mg–0.5Y–0.24O (wt.%) alloy under equilibrium conditions: **a** phase fractions shown up to 1% to reveal the minority phases, **b** distribution of solute Y between liquid and (Mg) phases

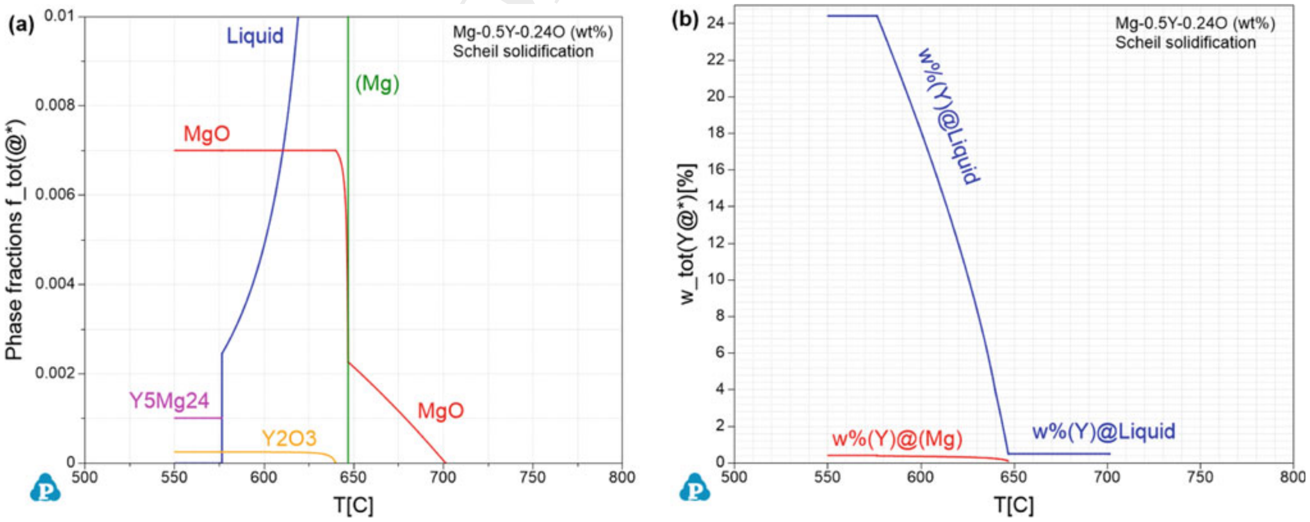

Fig. 5 Solidification simulation of the Mg-0.5Y-0.24O (wt.%) alloy under Scheil conditions: **a** phase fractions shown up to 1%, **b** distribution of solute Y between liquid and (Mg) phases; note that the average (total) wt.% of Y solute in (Mg) is plotted, ranging from 0.1 to 0.42 wt.% Y in the assumed layered growth of (Mg) under Scheil conditions

liquid alloy at the apex of the three-phase equilibrium Liquid + MgO + Y_2O_3 at 700 °C in Fig. 3b. Below 490 °C the solubility of Y at the three-phase equilibrium (Mg) + MgO + Y_2O_3 decreases as shown in Fig. 4b and the liberated Y forms Y_2O_3 at the cost of MgO in a solid-state reaction as given in Fig. 4a. The solubility of oxygen in (Mg) is negligibly small and both oxides MgO and Y_2O_3 are stoichiometric phases in this ternary system.

The results of solidification simulation of the same alloy under Scheil conditions, explained in Ref. [9], are given in Fig. 5. Initially the phase development in Fig. 5a is exactly the same as under equilibrium because there is no solid solution in the primary crystallizing MgO. At 647 °C the bulk of (Mg) starts crystallizing in the same monovariant eutectic reaction, Liquid → (Mg) + MgO. However, since back-diffusion of Y into the growing (Mg) phase is blocked the Y-enrichment in Liquid is huge, as shown in Fig. 5b. Below 640 °C Y_2O_3 starts growing while the phase fraction of MgO is frozen-in at 0.7%; the reaction switches to Liquid → (Mg) + Y_2O_3 until the ternary invariant eutectic reaction Liquid → (Mg) + Y_2O_3 + Y_5Mg_{24} terminates solidification at 576.4 °C. The solidified non-equilibrium constitution comprises four phases, the phase fractions are also plotted for better readability down to the arbitrary cut-off at 550°C in Fig. 5b: 99.17% (Mg) + 0.70% MgO + 0.10% Y_5Mg_{24} + 0.03% Y_2O_3. That is considered a good approximation of the as-cast microstructure of that alloy. The very small fraction of 0.1% Y_5Mg_{24} may be too small to be detected. Also, the initial alloy is certainly not single-phase Liquid at 700 °C but contains more oxygen in the form of MgO which was observed experimentally as highly dispersed native MgO particles after treatment by high shear melt conditioning before casting [1]. That phase fraction of MgO already present at 700 °C is simply added as inert basis to the MgO formed during the solidification simulations in Figs. 4a and 5a, at the cost of (Mg). This will reduce the tiny fraction of Y_5Mg_{24} even below 0.1%.

References

1. S. Wang, Y. Wang, Q.M. Ramasse, R. Schmid-Fetzer, Z. Fan, Segregation of Yttrium at the Mg/MgO interface in an Mg-0.5Y Alloy, Acta Materialia 257 (2023) 119147.
2. H. Men, Z. Fan, An Analytical Model for Solute Segregation at Liquid Metal/Solid Substrate Interface, Metallurgical and Materials Transactions A 45(12) (2014) 5508–5516.
3. O.B. Fabrichnaya, H.L. Lukas, G. Effenberg, F. Aldinger, Thermodynamic optimization in the Mg–Y system, Intermetallics 11(11) (2003) 1183–1188.
4. S.L. Chen, S. Daniel, F. Zhang, Y.A. Chang, X.Y. Yan, F.Y. Xie, R. Schmid-Fetzer, W.A. Oates, The PANDAT software package and its applications, Calphad 26(2) (2002) 175–188.
5. W. Cao, S.L. Chen, F. Zhang, K. Wu, Y. Yang, Y.A. Chang, R. Schmid-Fetzer, W.A. Oates, PANDAT software with PanEngine, PanOptimizer and PanPrecipitation for multi-component phase diagram calculation and materials property simulation, Calphad 33 (2) (2009) 328–342.
6. N. Eustathopoulos, Progress in understanding and modeling reactive wetting of metals on ceramics, Current Opinion in Solid State and Materials Science 9(4–5) (2005) 152–160.
7. M. Humenik Jr, W.D. Kingery, Metal-ceramic interactions: III, surface tension and wettability of metal-ceramic systems, Journal of the American Ceramic Society 37(1) (1954) 18–23.
8. S.-M. Liang, R. Schmid-Fetzer, Complete thermodynamic description of the Mg–Ca–O phase diagram including the Ca–O, Mg–O and CaO–MgO subsystems, Journal of the European Ceramic Society 38(14) (2018) 4768–4785.
9. R. Schmid-Fetzer, Phase Diagrams: The Beginning of Wisdom, Journal of Phase Equilibria and Diffusion 35(6) (2014) 735–760.